Research in Astronomy and Astrophysics, 24:085015 (6pp), 2024 August https://doi.org/10.1088/1674-4527/ad607d

Detection of Increasing γ-Ray Emissions from 4FGL J1718.5+4237 with Fermi-LAT

Jiao Zheng[1,2], Pengfei Zhang[1], and Li Zhang[1]
[1] Department of Astronomy, School of Physics and Astronomy, Key Laboratory of Astroparticle Physics of Yunnan Province, Yunnan University, Kunming 650091, China; zhangpengfei@ynu.edu.cn, lizhang@ynu.edu.cn
[2] School of Physics and Engineering Technology, Xingyi Normal University for Nationalities, Xingyi 562400, China
Received 2024 April 11; revised 2024 June 27; accepted 2024 July 4; published 2024 August 7

Abstract

We report a gradual brightening γ-ray source, 4FGL J1718.5+4237, in 0.1–500.0 GeV, which may be associated with a blazar NVSS J171822+423948 with a redshift of ∼2.7. We analyzed 15.25 yr of γ-ray data recorded by the Large Area Telescope on board the Fermi Gamma-ray Space Telescope and detected significant γ-ray emissions in the direction of the blazar with a test statistic (TS) of ∼135. Based on timing analysis using a 1 yr time bin, we have observed a gradual brightening in γ-ray emissions from the target. In our analysis, we categorize them into two states: Quiet (TS ∼ 0) and Loud (TS ∼ 226) states, with the distinction occurring in 2016 August (MJD 57602.69). From the Quiet state to the brightest period (the last data point), the γ-ray flux in 0.1–500.0 GeV increased by more than 12-fold from $<0.2\times10^{-8}$ photons cm^{-1} s^{-1} to 2.6×10^{-8} photons cm^{-1} s^{-1}. Additionally, we studied the spectral properties in detail for the Loud state and the overall data. While no significant variation was detected, both exhibited a spectral index Γ of ∼2.6. The origin of the brightening γ-ray emissions from the target is not yet clear. Future long-term multi-wavelength observations and studies will provide insight into the astrophysical mechanisms of the target.

Key words: galaxies: active – blazars: individual (4FGL J1718.5+4237)

1. Introduction

As the most luminous sources across the entire sky, active galactic nuclei (AGNs) are energetic astrophysical sources powered by accretion onto supermassive black holes in galaxies, and present unique observational signatures in which multi-wavelength electromagnetic spectral energy distributions (SEDs) extend from MHz radio frequencies to TeV γ-ray energies (Urry & Padovani 1995; Ulrich et al. 1997). The broadband SED from an AGN reveals a universal double broad hump structure in a $\log\nu-\log\nu F_\nu$ diagram, with the low-energy hump covering the radio to ultraviolet (UV) and X-ray frequencies, mostly due to synchrotron emission from electrons in a relativistic jet, while the origin of the high-energy hump from X-rays to γ-rays is highly debated. This component could be produced via inverse Compton (IC) scattering in the conventional leptonic emission scenario (e.g., Ghisellini et al. 1985; Begelman & Sikora 1987; Maraschi et al. 1992; Dermer & Schlickeiser 1993; Sikora et al. 1994; Bloom & Marscher 1996; Błażejowski et al. 2000; Finke et al. 2008; Ghisellini & Tavecchio 2009; Abdo et al. 2010a; Kang et al. 2014; Yan et al. 2014) or could be either via proton synchrotron emission inside the jet (e.g., Mücke & Protheroe 2001) or secondary particles in electromagnetic cascades initiated by pion decay in the hadronic emission scenario (e.g., Mannheim & Biermann 1992; Aharonian 2000; Mücke & Protheroe 2001; Mücke et al. 2003; Böttcher et al. 2013; Petropoulou & Mastichiadis 2015; Gasparyan et al. 2022). It is general believed that AGNs are classified as different subclasses based on their observational characteristics and physical properties.

The Large Area Telescope on board the Fermi Gamma-ray Space Telescope (Fermi-LAT; Atwood et al. 2009) monitors the entire high-energy γ-ray sky every three hours, which affords us an ideal opportunity to investigate the γ-ray emissions from AGNs, unbiased by activity state or AGN sub-class. This ability has revealed the AGNs are dominant sources in the extragalactic γ-ray sky. In the Fourth Fermi-LAT Source catalog (4FGL-DR4; Ballet et al. 2023), about 4015 AGNs were published with energy >100 MeV, accounting for more than 55% of all Fermi-LAT sources. Among them, blazars, a subclass of AGNs with powerful relativistic jets oriented at small angles ($\leqslant10^\circ$) with respect to the line of sight to the observer (Urry & Padovani 1995), are the most abundant proportion of known γ-ray AGNs (Ballet et al. 2023). Blazars are typically subdivided into flat spectrum radio quasars (FSRQs), which display strong emission line components in the optical spectrum, and BL Lacertae objects (BL Lacs) that have weak or no emission lines (Urry & Padovani 1995). Among Fermi blazars, BL Lacs and FSRQs account for ∼40% and ∼20% of the sources, respectively, while blazar candidates of unknown types are about 35% of all Fermi blazars (3LAC;

Ajello et al. 2022). So far, a handful of γ-ray blazars have been even found at very high-redshifts ($z > 2$) (e.g., Romani et al. 2004; Abdo et al. 2010b; Ackermann et al. 2015, 2017; Paliya 2015; Ajello et al. 2016, 2022; Paliya et al. 2016, 2019; Kaur et al. 2017, 2018; Liao et al. 2018; Sahakyan et al. 2020), and one of the major characteristics of these sources is that they have softer γ-ray spectra. Here we present the γ-ray emissions of 4FGL J1718.5+4237 from 4FGL-DR4 (Ballet et al. 2023), which may be associated with a blazar, NVSS J171822 +423948, with a redshift of ∼2.7.

Zhang et al. (2023) carried out an analysis for γ-rays from the globular cluster NGC 6341 with Fermi-LAT, and found a significant γ-ray excess presented with a maximum likelihood test statistic (TS) of ∼40 (see their paper for more details). Motivated by their findings, we conducted a detailed data analysis for ∼15.25 yr Fermi-LAT observations on the γ-ray excess and discovered a high-energy γ-ray emission counterpart of a blazar, NVSS J171822+423948, exhibiting increasingly bright features in GeV γ-rays. Jiang et al. (2024) claimed that it is co-spatial with the IceCube neutrino event IC-201221A. This paper is structured as follows. In Section 2, we describe the Fermi-LAT data analysis procedures used in this work and report the γ-ray results. We summarize and discuss some results in Section 3.

2. Fermi-LAT Data Analysis

In Zhang et al. (2023), a new γ-ray source at R. A. $= 17^{\rm h}18^{\rm m}29\overset{\rm s}{.}79$ and decl. $= +42°38'37\overset{''}{.}38$ was found with a TS value of ∼40, then it was cataloged as 4FGL J1718.5 +4237 in 4FGL-DR4 based on Fermi-LAT 14 yr data (Ballet et al. 2023). We then carried out a data analysis for 4FGL J1718.5+4237 with Fermi-LAT 15.25 yr data. Using the tool *gtfindsrc*, we derived the position of 4FGL J1718.5+4237 at R. A. $= 17^{\rm h}18^{\rm m}26\overset{\rm s}{.}88$ and decl. $= +42°38'30\overset{''}{.}46$ with a 68% confidence level error radius of $2\overset{'}{.}1$. The following analyses are based on this γ-ray position. To identify the origin of the γ-ray source, we carefully cross-checked all possible γ-ray sources within $3\overset{'}{.}5$ (2σ error circle) around 4FGL J1718.5+4237 in Simbad database,[3] and totally retrieved eight objects including a blazar named NVSS J171822+423948 (Gaia Collaboration 2020) with optical position of R. A. $= 17^{\rm h}18^{\rm m}22\overset{\rm s}{.}77$ and decl. $= +42°39'45\overset{''}{.}05$ with angular distance of $1\overset{'}{.}5$ from the γ-ray position. We further investigated these sources with the NASA/IPAC Extragalactic Database (NED),[4] and excluded other known possible γ-ray sources that are not found to be potential γ-ray emitters. The nearest known γ-ray source in the 4FGL-DR4, 4FGL J1716.8+4310 (R. A. $= 259\overset{\circ}{.}203$, decl. $= +43\overset{\circ}{.}173$) associated with the γ-ray counterpart of globular cluster NGC 6341, is about $0\overset{\circ}{.}58$ away. Therefore, the most likely counterpart of the γ-ray source 4FGL J1718.5 +4237 would be NVSS J171822+423948, although we still cannot conclusively rule out the other sources within the 2σ error circle of γ-ray position. The following data analysis is aiming to determine the association between this γ-ray source and NVSS J171822+423948.

2.1. Data Reduction and Best-fit Model

The data utilized in the current study comprise all-sky-survey observations taken during 15.25 yr of Fermi-LAT operation, from 2008 August 4 (MJD 54682.6) to 2023 November 1 (MJD 60249.3). The LAT Pass 8 *Front + Back* (evclass = 128 and evtype = 3) "Source" class events in the energy range 0.1–500.0 GeV were extracted from a $20° \times 20°$ region of interest (RoI) centered on the γ-ray position by the used Fermi Science Tools software package of Fermitools2.0.19. The events with zenith angles >90° were filtered out to avoid the γ-ray contamination from the Earth's limb. The expression "DATA_QUAL>0 && LAT_CONFIG = 1" was selected to obtain the good time intervals by employing the tool *gtmktime*. The instrument response function of "P8R3_SOURCE_V3" was adopted.

We used a script named make4FGLxml.py[5] to generate a model file, which consists of γ-ray sources within the RoI of the 4FGL-DR4 catalog. The model file included the spectral parameters, the spectral forms, and the coordinates for γ-ray sources in the 4FGL-DR4 within 25° around 4FGL J1718.5+4237. These initial values were derived from the catalog file of gll_psc_v34.fit.[6] The latest diffuse emission templates of gll_iem_v07.fits and iso_P8R3_SOURCE_V3_v1.txt were used to model the two γ-ray backgrounds of the Galactic and extragalactic isotropic emissions,[7] respectively. In the data analysis, the parameters of the flux normalizations and the spectral shapes were set free for the sources within 5°. While for the sources within 5°–10° or those outside 10° but identified as variable sources, we also freed their flux normalizations. The normalizations of the two backgrounds were set free too. We froze all other parameters at their values that were provided in 4FGL-DR4. For 4FGL J1718.5+4237, its γ-ray spectrum is described by a power-law (PL) spectral shape of $dN/dE = N_0(E/E_0)^{-\Gamma}$ with the spectral index $\Gamma = 2.5$.

Then we performed a binned maximum likelihood analysis between the whole database and the model file. The data reduction followed the standard criteria for the point-source analysis that is recommended by Fermi-LAT Collaboration.[8] The fit for 4FGL J1718.5+4237 results in TS ∼ 135 in the 0.1–500.0 GeV energy range, with an integrated average

[3] https://simbad.u-strasbg.fr/simbad/
[4] http://ned.ipac.caltech.edu/
[5] https://fermi.gsfc.nasa.gov/ssc/data/analysis/user/
[6] https://fermi.gsfc.nasa.gov/ssc/data/access/lat/14yr_catalog/
[7] https://fermi.gsfc.nasa.gov/ssc/data/access/lat/BackgroundModels.html
[8] https://fermi.gsfc.nasa.gov/ssc/data/analysis/scitools/

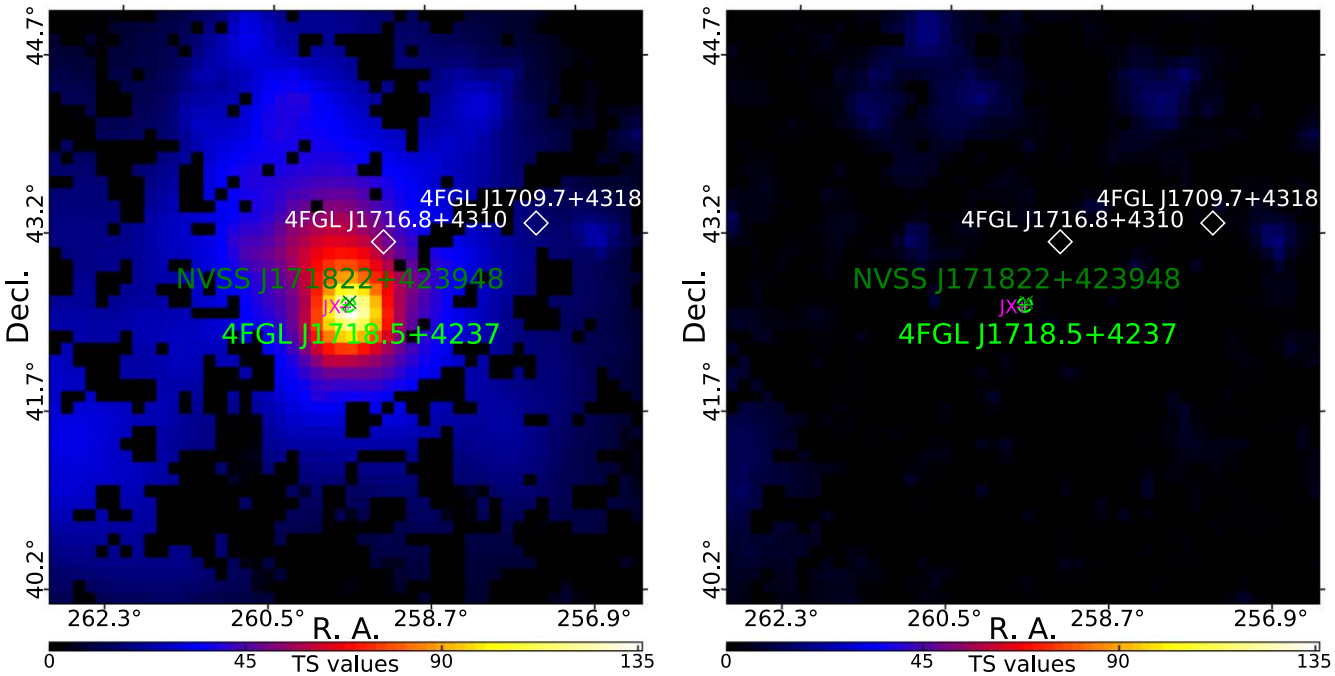

Figure 1. TS map (left) and residual TS map (right) with a $5^\circ \times 5^\circ$ region around 4FGL J1718.5+4237 in 0.1–500.0 GeV obtained with ∼15.25 yr of Fermi-LAT data. The coordinate of NVSS J171822+423948 is marked with a green cross. The γ-ray source 4FGL J1718.5+4237 is tagged with a lime plus, and the lime circle stands for 2σ error circle of target. The position of 4FGL J1718.5+4237 reported in Jiang et al. (2024) is tagged with a purple plus (marked with "JX"). Other 4FGL-DR4 γ-ray sources that begin with "4FGL" are shown with white diamonds. The TS value at each pixel on the sky is scaled with color. The two TS maps share the same color-bar for convenient comparison and have a spatial pixel size of $0.^\circ1 \times 0.^\circ1$ on one side.

Table 1
Best-fit Results of the Likelihood Analysis for 4FGL J1718.5+4237

Time Range (MJD)	Model	Parameter Value			
	PL	Γ	TS	Flux	
54682.6−60249.3	(Whole)	2.60(0.10)	135.09	6.80(1.30)	
		2.50(0.12)[a]	…	…	
54682.6−57602.7	(Quiet)	…	0.0	2.12[b]	
57602.7−60249.3	(Loud)	2.55(0.08)	226.25	11.92(1.72)	
	LP	α	β	E_b (GeV)	TS
	(Loud)	2.55(0.14)	0.13(0.07)	1.17	219.45

Notes. The integrated photon flux is in the unit 10^{-9} photons cm^{-2} s^{-1}, and the errors are in parentheses.
[a] Parameter values of PL model provided in 4FGL-DR4,
[b] The 95% (2σ) flux upper limit.

photon flux of $(6.80 \pm 1.30) \times 10^{-9}$ photons cm^{-2} s^{-1} and a photon index of $\Gamma \sim 2.6$. Its parameter values are in good agreement with those reported in 4FGL-DR4, except for the TS value. The best-fit results of the likelihood analysis for the target are listed in Table 1. The SEDs of AGNs in MeV-GeV ranges can also be described by a log-parabola (LP) model with a formula of $dN/dE = N_0(E/E_b)^{-(\alpha+\beta\log(E/E_b))}$ (e.g., Cerruti et al. 2013; Dermer et al. 2014, 2015). We also fitted the events with a spectrum of an LP model, and the best-fit results for the LP model are also shown in Table 1. Comparing the best-fit results of the two models, we believe that PL is the best model for the target. Then the best-fit results of the PL model were saved as a new model file.

Based on the new model, we employed the tool *gttsmap* to calculate a $5^\circ \times 5^\circ$ TS map centered at 4FGL J1718.5+4237 in the energy range of 0.1–500.0 GeV. In this step, we removed the target in the model file. All the parameters of the γ-ray sources in the RoI, except the two diffuse components, were fixed at the values from the best-fit model. The TS map is displayed in the left panel of Figure 1. We mark the 4FGL J1718.5+4237 and NVSS J171822+423948 with a lime plus and a green cross, respectively. The lime circle stands for 2σ

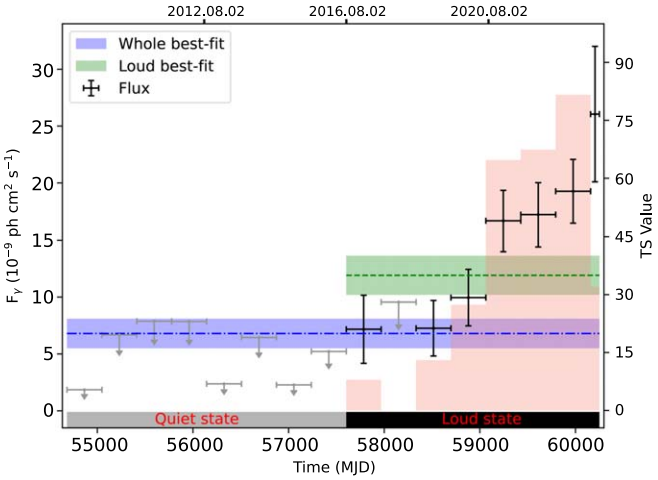

Figure 2. The ∼15.25 yr integrated flux of 4FGL J1718.5+4237 in 0.1–500.0 GeV using a PL model with 1 yr time bins. The data points represent the source photon flux for time bins with TS > 5, and their TS values are displayed with pink bars. For TS < 5, we derived 95% flux upper limits, which are shown with gray arrows. The mean flux and the corresponding uncertainty range from the whole likelihood analysis are marked with a horizontal blue dash-dotted line and a blue shade, respectively. The fluxes and uncertainties of the Loud state are marked with a green dashed line and a green shade, respectively. Note that the last data point only covers 0.25 yr.

error circle of the γ-ray position of 4FGL J1718.5+4237. In order to examine contamination from the nearby potential γ-ray source (not included in 4FGL-DR4), a residual TS map was obtained based on the above best-fit model. The residual TS map is featured in the right panel of Figure 1. We found that no pixel having TS > 25 is seen in the residual TS map.

2.2. Long-term Flux Variability

To investigate the temporal variability behavior in GeV, we constructed a light curve for the target in 0.1–500.0 GeV by performing an unbinned likelihood analysis based on the new model file. In order to show the light curve as completely as possible and to facilitate future comparisons between our data and others' results, the yearly binning method is used in this step. Here, we fixed the parameters of spectral shapes at their best-fit values and only freed the normalizations mentioned above for the sources in the RoI. We presented the flux and the corresponding TS value for each time bin in Figure 2. The data points with TS > 5 were included to show the light curve as completely as possible. Otherwise we derived their 95% flux upper limits for the data points with TS < 5 and colored them gray. Additionally, it should be noted that the last data point is incomplete, covering only 3 months. From Figure 2, we know that the target's γ-ray emissions are mainly concentrated in the latter part, reaching its maximum γ-ray flux state in the last time bin recorded so far.

2.3. Quiet and Loud States

According to Figure 2, we defined the time period as two distinctive emission states: Quiet and Loud states, marked with gray and black shades in Figure 2, respectively. A Loud state refers to the period of detection of high flux from 2016 August (MJD 57602.69) to the end of the data, and a Quiet state is selected as the time period when the source is in a relatively fainter state from 2008 August to 2016 August. We also carried out the likelihood analysis for the two states. For the Quiet state, we obtained the TS value of 0 and a flux upper limit of $\sim 2.12 \times 10^{-9}$ photons cm^{-2} s^{-1}, and the Loud state results in TS = 226, and the flux is $\sim 1.19 \times 10^{-8}$ photons cm^{-2} s^{-1} with $\Gamma \sim 2.6$ in 0.1–500.0 GeV. The results are presented in Table 1. The index Γ is consistent with them in the whole fit result, which suggests that no spectral variation occurs during the Loud state. All the best-fit results were saved as two updated model files, which will be used in the next procedure of the analysis.

Based on two updated models, we created $5^\circ \times 5^\circ$ TS maps for the two states, respectively. They are shown in the left and right panels of Figure 3. These two TS maps used the one color bar to scale their TS values for each grid location on the sky.

2.4. Spectral Analysis in Loud State

To investigate the spectral shape in 0.1–500.0 GeV during the Loud state, we constructed its SED based on the updated model. We fixed the parameters of spectral shape for all the sources at their best-fit values and only freed the normalizations of the target and two backgrounds. We divided the 0.1–500.0 GeV energy band into 12 equally logarithmically spaced energy bins, and then performed the likelihood analysis to calculate the flux and TS values for each energy bin. The γ-ray data points with TS > 5 are represented in Figure 4 with black marks, otherwise 95% upper limits of flux are shown with gray marks. The PL best-fit model is displayed with a blue solid line.

The LP model was also used to fit the γ-ray events from the target. We obtain a spectral slope $\alpha \sim 2.6$, a curvature parameter around the peak $\beta \sim 0.13$, and a TS ∼ 220 (listed in Table 1). We show them in Figure 4 with an orange dash-dotted line. A likelihood ratio test was used to check the PL model (null hypothesis) against the LP model (alternative hypothesis). We compared these values by defining the curvature test statistic $\mathrm{TS}_{\mathrm{curve}} = 2\log(\mathcal{L}_{\mathrm{LP}}/\mathcal{L}_{\mathrm{PL}})$ (Nolan et al. 2012), and the $\mathrm{TS}_{\mathrm{curve}}$ was calculated to be ~ -3. This maybe indicates no statistical evidence for a curved spectral shape. From Figure 4, we also can see that the PL model gives an acceptable description for the SED, which agrees well with the whole fitting.

3. Results and Discussion

In this work, we present the preliminary results of our study on 4FGL J1718.5+4237 in the latest release of LAT source catalog 4FGL-DR4 (Ballet et al. 2023) using the Fermi-LAT

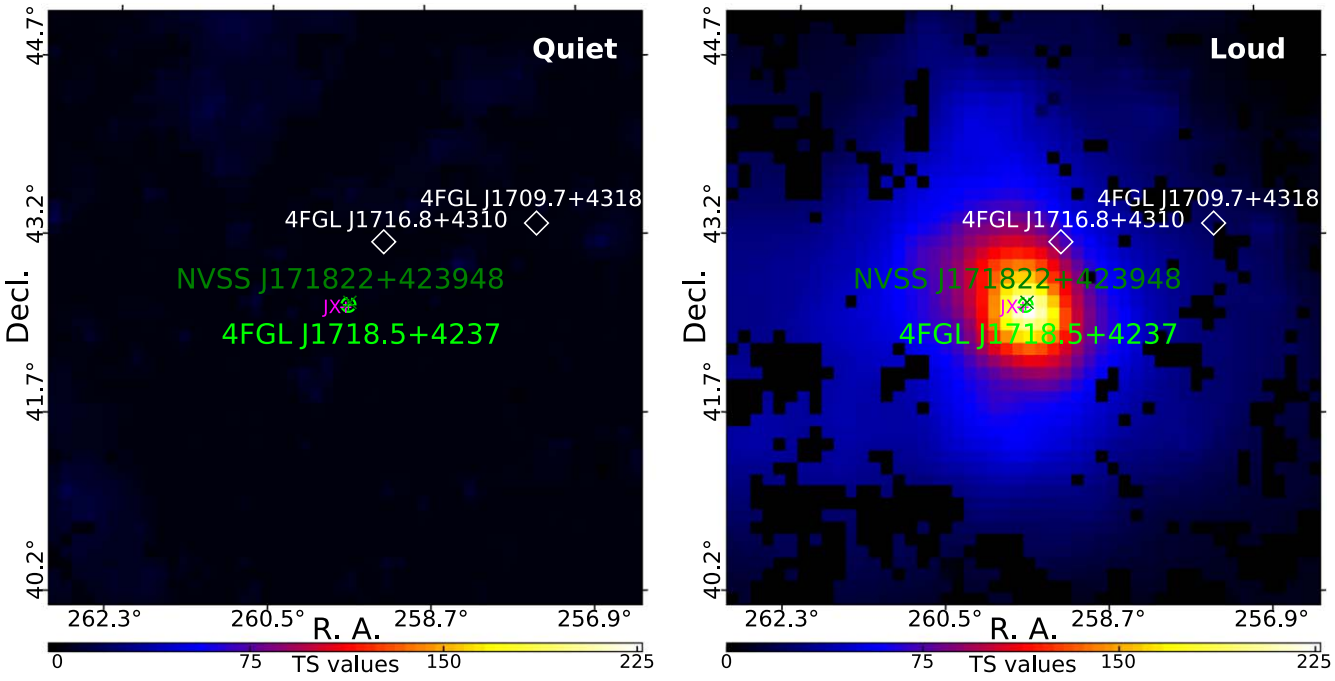

Figure 3. Two TS maps in the left and right panels are obtained with the events from Quiet and Loud states, respectively. Other aspects are the same as in Figure 1.

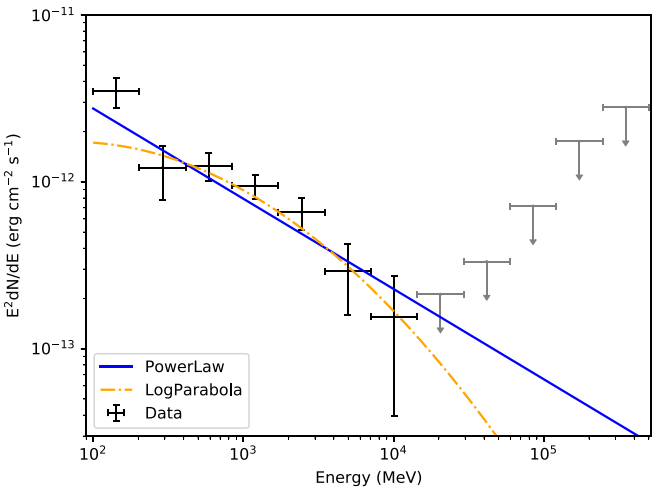

Figure 4. 0.1–500.0 GeV SED of 4FGL J1718.5+4237 in the Loud state. The 95% flux upper limit is calculated for the data points with TS < 5. The blue solid and orange dash-dotted lines represent the best-fit results of PL and LP models, respectively.

Pass 8 data set covering 15.25 yr from 2008 August to 2023 November in the energy range 0.1–500.0 GeV, and it was detected at a significance level of $\sim 11.6\sigma$. This γ-ray source is positionally associated with the blazar NVSS J171822+423948 at a high-redshift of ~ 2.7. Our results suggested that NVSS J171822+423948 is a new γ-ray emitter and has remained in quiescence for a long time. In the derived TS maps (see Figure 1), the position of NVSS J171822+423948 falls into the 1σ error circle of 4FGL J1718.5+4237 in γ-rays. The angular separation between the optical and γ-ray coordinates is derived as $1\farcs5$. This observation provides further evidence of NVSS J171822+423948 being a new γ-ray emitter in the extragalactic high-energy sky.

From the long-term light curve, interestingly, the source showed a significant increase in γ-ray flux and continuous brightening since approximately MJD 57602.69 (date 2016 August 2 16:29:16.8 UTC). We performed a spectral analysis of the γ-ray emissions from NVSS J171822+423948 during the Loud state. The results are listed in Table 1 and the SED is displayed in Figure 4. The γ-ray spectrum is well described by a PL model. The γ-ray flux in the brightest period (the last data point) increased as much as ~ 12 orders of magnitude compared to the flux upper limit in the Quiet state (estimated over 8 yr of Fermi-LAT observations). Its γ-ray spectrum is soft, which aligned with that typically observed from high-redshift blazars ($z > 2$) (e.g., Ackermann et al. 2015).

In the previous literatures (Véron-Cetty & Véron 2006, 2010; Ahn et al. 2012; Gaia Collaboration 2020), they presented a compilation of all known AGNs, and NVSS J171822+423948 was one entry in the catalog and classified as a blazar. In Zhang et al. (2023), a significant γ-ray excess with a TS of ~ 40 was presented in their results, but they did not provide much discussion on this source. It was subsequently cataloged in 4FGL-DR4 (Ballet et al. 2023). Jiang et al. (2024), reported on the multi-wavelength and multi-messenger studies of this blazar, including its γ-ray emissions, and claimed that

this blazar is the low-energy counterpart of 4FGL J1718.5 +4237. They also stated that 4FGL J1718.5+4237 is the only gamma-ray source known to be co-spatial with the IceCube neutrino event IC-201221A with an arrival time at MJD 59204, which corresponds to 2020 December 21. This will be very important for the study of high-energy neutrino astronomy. Their analysis of LAT data extends up to MJD 59945 (2023 January 1). Moreover, this γ-ray source exhibited no variation in its GeV light curves from MJD 58856 (2020 January 8) to 59945 (2023 January 1). Here, we extend the time range of the data analysis and found a trend of gradually increasing gamma-ray emissions from 4FGL J1718.5+4237 starting from MJD 58333 (2018 August 2). Therefore, further multi-wavelength observing campaigns for NVSS J171822+423948 are strongly encouraged, which will be important to reveal the properties of this high-redshift blazar. Particularly, carrying out optical and X-ray observations of this γ-ray source during the Loud state will enable us to compare the broadband SED and constrain the underlying astrophysical mechanisms.

Acknowledgments

We thank an anonymous referee for the comments that helped improve this work. This work is supported in part by the National Natural Science Foundation of China (NSFC, grant Nos. 12233006 and 12163006), the Basic Research Program of Yunnan Province No. 202201AT070137, and the joint foundation of Department of Science and Technology of Yunnan Province and Yunnan University No. 202201BF070001-020. P. F. Zhang acknowledges the support by the Xingdian Talent Support Plan—Youth Project.

Data Availability

The data underlying this work can be made available in the Fermi Science Support Center.[9]

References

Abdo, A. A., Ackermann, M., Agudo, I., et al. 2010a, ApJ, 716, 30
Abdo, A. A., Ackermann, M., Ajello, M., et al. 2010b, ApJ, 715, 429
Ackermann, M., Ajello, M., Atwood, W. B., et al. 2015, ApJ, 810, 14
Ackermann, M., Ajello, M., Baldini, L., et al. 2017, ApJL, 837, L5
Aharonian, F. A. 2000, NewA, 5, 377
Ahn, C. P., Alexandroff, R., Allende Prieto, C., et al. 2012, ApJS, 203, 21
Ajello, M., Baldini, L., Ballet, J., et al. 2022, ApJS, 263, 24
Ajello, M., Ghisellini, G., Paliya, V. S., et al. 2016, ApJ, 826, 76
Atwood, W. B., Abdo, A. A., Ackermann, M., et al. 2009, ApJ, 697, 1071
Ballet, J., Bruel, P., Burnett, T. H., Lott, B. & The Fermi-LAT collaboration 2023, arXiv:2307.12546
Begelman, M. C., & Sikora, M. 1987, ApJ, 322, 650
Błażejowski, M., Sikora, M., Moderski, R., & Madejski, G. M. 2000, ApJ, 545, 107
Bloom, S. D., & Marscher, A. P. 1996, ApJ, 461, 657
Böttcher, M., Reimer, A., Sweeney, K., & Prakash, A. 2013, ApJ, 768, 54
Cerruti, M., Dermer, C. D., Lott, B., Boisson, C., & Zech, A. 2013, ApJL, 771, L4
Dermer, C. D., Cerruti, M., Lott, B., Boisson, C., & Zech, A. 2014, ApJ, 782, 82
Dermer, C. D., & Schlickeiser, R. 1993, ApJ, 416, 458
Dermer, C. D., Yan, D., Zhang, L., Finke, J. D., & Lott, B. 2015, ApJ, 809, 174
Finke, J. D., Dermer, C. D., & Böttcher, M. 2008, ApJ, 686, 181
Gaia Collaboration 2020, yCat I/350
Gasparyan, S., Bégué, D., & Sahakyan, N. 2022, MNRAS, 509, 2102
Ghisellini, G., Maraschi, L., & Treves, A. 1985, A&A, 146, 204
Ghisellini, G., & Tavecchio, F. 2009, MNRAS, 397, 985
Jiang, X., Liao, N.-H., Wang, Y.-B., et al. 2024, ApJL, 965, L2
Kang, S.-J., Chen, L., & Wu, Q. 2014, ApJS, 215, 5
Kaur, A., Rau, A., Ajello, M., et al. 2018, ApJ, 859, 80
Kaur, A., Rau, A., Ajello, M., et al. 2017, ApJ, 834, 41
Liao, N.-H., Li, S., & Fan, Y.-Z. 2018, ApJL, 865, L17
Mannheim, K., & Biermann, P. L. 1992, A&A, 253, L21
Maraschi, L., Ghisellini, G., & Celotti, A. 1992, ApJL, 397, L5
Mücke, A., & Protheroe, R. J. 2001, APh, 15, 121
Mücke, A., Protheroe, R. J., Engel, R., Rachen, J. P., & Stanev, T. 2003, APh, 18, 593
Nolan, P. L., Abdo, A. A., Ackermann, M., et al. 2012, ApJS, 199, 31
Paliya, V. S. 2015, ApJ, 804, 74
Paliya, V. S., Ajello, M., Ojha, R., et al. 2019, ApJ, 871, 211
Paliya, V. S., Parker, M. L., Fabian, A. C., & Stalin, C. S. 2016, ApJ, 825, 74
Petropoulou, M., & Mastichiadis, A. 2015, MNRAS, 447, 36
Romani, R. W., Sowards-Emmerd, D., Greenhill, L., & Michelson, P. 2004, ApJL, 610, L9
Sahakyan, N., Israyelyan, D., Harutyunyan, G., Khachatryan, M., & Gasparyan, S. 2020, MNRAS, 498, 2594
Sikora, M., Begelman, M. C., & Rees, M. J. 1994, ApJ, 421, 153
Ulrich, M.-H., Maraschi, L., & Urry, C. M. 1997, ARA&A, 35, 445
Urry, C. M., & Padovani, P. 1995, PASP, 107, 803
Véron-Cetty, M. P., & Véron, P. 2010, A&A, 518, A10
Véron-Cetty, M. P., & Véron, P. 2006, A&A, 455, 773
Yan, D., Zeng, H., & Zhang, L. 2014, MNRAS, 439, 2933
Zhang, P., Xing, Y., Wang, Z., Wu, W., & Chen, Z. 2023, ApJ, 945, 70

[9] https://heasarc.gsfc.nasa.gov/FTP/fermi/data/lat/weekly/photon/